Bulletin of the JSME Vol.11, No.3, 2016
Journal of Fluid Science and Technology

Validation scheme for small effect of wind tunnel blockage on decaying grid-generated turbulence

Hiroki SUZUKI*, Shinsuke MOCHIZUKI* and Yutaka HASEGAWA**
* Graduate School of Sciences and Technology for Innovation, Yamaguchi University
2-16-1 Tokiwa-dai, Ube-shi, Yamaguchi 755-8611, Japan
E-mail: h.suzuki@yamaguchi-u.ac.jp
** Department of Electrical and Mechanical Engineering, Nagoya Institute of Technology
Gokiso-cho, Showa-ku, Nagoya-shi, 466-8555, Japan

Received 21 March 2016

Abstract
This paper proposes a validation scheme for the effect of wind tunnel blockage on decaying grid-generated turbulence. This validation scheme was derived from the governing equations of the k–ϵ model. Analytical solutions for the validation scheme were derived by introducing a model of the difference between the rate of change of the effect of fluid acceleration on the turbulent kinetic energy and that of the effect on its dissipation. The derived solutions include a decay exponent that excludes the acceleration effect, a parameter characterizing the acceleration, the initial anisotropy, and the model coefficient of the k–ϵ model, and can be quantified by parameters which can be known. The physical meaning of the model was clarified. The derived solutions and model were confirmed to be accurate through numerical simulation. An equation for the decay exponent, which is also affected by the fluid acceleration, was developed using the derived solutions. This scheme was applied to the examination of the reduced fluid acceleration effect in a moderate-sized wind tunnel to measure the grid-generated turbulence. The fluid acceleration effect in the wind tunnel was confirmed to be small using the derived equations. The decay characteristics of the grid-generated turbulence in the wind tunnel were measured and were found to agree with those obtained in previous experiments.

Key words : Turbulent flow, Wind tunnel blockage, Grid-generated turbulence, k–ϵ model

1. Introduction

Decaying homogeneous turbulence is a common occurrence in mechanical engineering applications. In this type of turbulent flow, the turbulent kinetic energy decreases as a result of viscous dissipation. In experimental observations, grid-generated turbulence, which is generated by a turbulence-generating grid placed in a uniform flow, is used to study decaying turbulence. Grid-generated turbulence has been used to experimentally study decaying turbulence (e.g., Comte-Bellot and Corrsin, 1966; Bennett and Corrsin, 1978; Mohamed and LaRue, 1990; Lavoie et al., 2005; Lavoie et al., 2007; Kurian and Fransson, 2009; Krogstad and Davidson, 2010; Valente and Vassilicos, 2012; Nagata et al., 2013). Grid-generated turbulence has also been numerically simulated in recent studies (e.g., Suzuki et al., 2010; Suzuki et al., 2013). The decreasing turbulent kinetic energy in a fully developed grid-generated turbulence is described by a power law in the downstream region. This power law, which has the same form as that used to describe decaying turbulent kinetic energy, is obtained by applying a self-preserving form to the transport equation of the velocity correlation function and includes a decay exponent and a decay coefficient. The decay coefficient is related to the drag coefficient of the turbulence-generating grid when the decay exponent is unity (Hinze, 1975); under this condition, the power law is referred to as the linear decay law.

The decay exponent n has been investigated in several previous works. Although theoretical studies have indicated that the decay exponent can take values of $n = 1$, 6/5, and 10/7 under high-Reynolds number flow in homogeneous isotropic turbulence, as shown in a histogram of the distribution of the decay exponent in Meldi and Sagaut (2012), rather large variation in the decay exponent has been observed, and most experimental values do not agree with the theoretical

Paper No.16-00195
[DOI: 10.1299/jfst.2016jfst0012]

predictions. A figure in Sinhuber et al. (2015) demonstrates the particularly large variation in the value of the decay exponent at moderate Reynolds numbers. This observation has also been reported in other previous works (e.g., Davidson, 2011). George (1992) noted that n depends on the initial conditions because the Reynolds number is finite.The potential effects of inflow conditions on the decay characteristics of decaying homogeneous turbulence have been investigated in previous experiments (Lavoie et al., 2007; Valente and Vassilicos, 2012). The variation of the dissipation coefficient was used to determine this variation (Krogstad and Davidson, 2010; Davidson, 2011). The decay exponent has also been considered with regard to the engineering modeling of flows. For instance, in k–ϵ modeling, the model coefficient $C_{\epsilon 2}$ is defined as a function of the decay exponent as $C_{\epsilon 2} = (n + 1)/n$ (Pope, 2000). For decay exponents in the range of $n = 1.15$–1.45, the model coefficient varies in the range of $C_{\epsilon 2} = 1.69$–1.87, although the standard value is $C_{\epsilon 2} = 1.92$.

In wind tunnels used for experiments on grid-generated turbulence, the effective cross-sectional area is finite and can decrease as a result of the development of a boundary layer on the side walls. Previous studies have investigated the effect of turbulent boundary layers developing on the side walls on decaying turbulence at small Reynolds numbers (e.g., Bennett and Corrsin, 1978). The effect of missing large scales in the experimental and numerical analysis because of the finite size of the domain on the determination of the integral scale has also been studied (Wang and George, 2002). Reducing the area of the wind tunnel may cause fluid acceleration, which affects the turbulent kinetic energy. The effect of fluid acceleration due to wind tunnel blockage has received attention in experiments on grid-generated turbulence. In past experiments, the side walls of the wind tunnel have been carefully adjusted to reduce the acceleration effect (Lavoie et al., 2007; Krogstad and Davidson, 2010).

This careful attention to the fluid acceleration effect can also be also found in experiments on turbulent boundary layers with a zero pressure gradient (Osaka et al., 1998; de Graaff and Eaton, 2000; Schultz and Flack, 2003; Schultz and Flack, 2007; Volino et al., 2009; Volino et al., 2011; Örlü and Schlatter, 2013). The acceleration of the free stream can be reduced to produce a turbulent boundary layer with a negligible pressure gradient. The magnitude of the fluid acceleration is characterized by the acceleration parameter. In the abovementioned experiments, the value of the parameter was set to be smaller than 1.6×10^{-6} (de Graaff and Eaton, 2000).

Few studies have attempted to quantify the effect of acceleration due to wind tunnel blockage on decaying grid-generated turbulence. Most previous experiments have used a small or moderate-sized wind tunnel (Barlow et al., 1999). An increased contraction ratio improves the uniformity of the incoming flow and reduces background velocity fluctuation. Increasing the contraction ratio while maintaining a constant wind tunnel size decreases the cross-sectional area of the wind tunnel, which causes the magnitude of the fluid acceleration to increase. Although the range of acceptable fluid accelerations should be known, few studies have addressed the relationship between the magnitude of the fluid acceleration and the acceleration effect in comparison with the number of previous experiments on turbulent boundary layers. Because the range of acceptable fluid accelerations depends on the experimental conditions, a formula describing the range of acceptable values of the acceleration effect should be derived.

In this study, a validation scheme for the effect of fluid acceleration due to wind tunnel blockage on decaying grid-generated turbulence was devised. The governing equations of the k–ϵ model (Pope, 2000) were used to develop the scheme, and governing equations describing the effect of the fluid acceleration on the turbulent kinetic energy and its dissipation were derived. An analytical solution, which is an approximation of the numerical solution, was then derived and validated against numerical simulation results. Using the analytical solution, the decay exponent, which is affected by the fluid acceleration, were also derived. The effect of the uncertainty of the model coefficient is also discussed in terms of the analytical solution. Using the derived analytical solution, the reduced fluid acceleration effect in a moderate-sized wind tunnel was examined and quantified. Specifically, the effect of the acceleration on the turbulent kinetic energy, its dissipation, and the decay exponent were quantified. The acceleration parameter was measured and was found to be comparable to those obtained in previous experiments. The absolute relative magnitude of the acceleration effect on the decaying grid-generated turbulence in the present wind tunnel was confirmed to be small. The decay characteristics of the grid-generated turbulence in the validated wind tunnel were measured.

The remainder of this paper is organized as follows. Section 2 presents the derivation of the governing equations of the fluid acceleration effect from those of the k–ϵ model framework. The simulated equations are discussed to show the effect of fluid acceleration due to wind tunnel blockage. Section 3 presents the derivation of the analytical solution for the validation scheme and its validation against the numerical results with some issues of discussion. In Section 4, the validation scheme is used to validate the wind tunnel blockage effect in a moderate-sized wind tunnel, and the decaying grid-generated turbulence in the wind tunnel is measured. Section 5 concludes the paper.

[DOI: 10.1299/jfst.2016jfst0012]

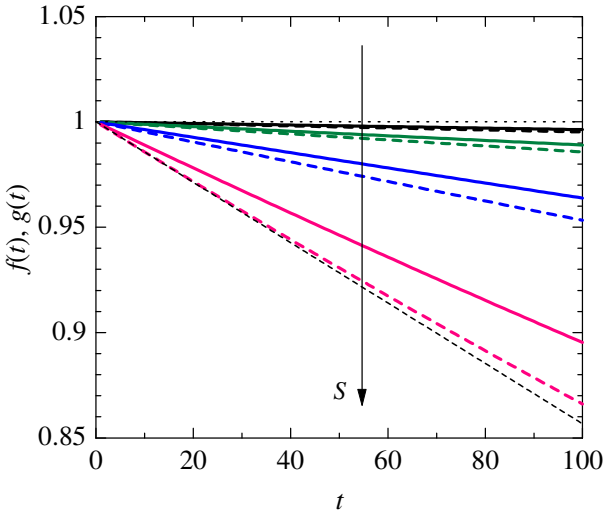

Fig. 1 Temporal evolutions of $f(t)$ and $g(t)$ at $a = 0.5$ and $n = 1.2$. Black, green, blue, and red lines show results at $S = 1 \times 10^{-4}$, 3×10^{-4}, 1×10^{-3}, and 3×10^{-3}, respectively. Solid and dashed lines represent $f(t)$ and $g(t)$, respectively. The deviations of $f(t)$ and $g(t)$ increased with increasing S. The thin dashed line shows a linear function with a slope equal to the initial gradient $\mathrm{d}g/\mathrm{d}t|_{t=0}$ of $g(t)$. The deviation of $g(t)$ from this linear function indicates that $g(t)$ is nonlinear. The fluid acceleration effect reduces the influence functions. The influence function $g(t)$ of the dissipation was more sensitive to changes in the fluid acceleration than that of $f(t)$ of the turbulent kinetic energy.

2. Numerical simulation

2.1. Governing equations

An axisymmetric homogeneous turbulence was analyzed in this study because a homogeneous turbulence with a uniform convection velocity is similar to grid-generated turbulence. Additionally, the fluid acceleration considered in this study was weak. For this analysis, the framework of the k–ϵ model was introduced. The governing equations of the k–ϵ model for a homogeneous turbulence are generally given as follows (Pope, 2000):

$$\frac{\mathrm{d}k}{\mathrm{d}t'} = P - \epsilon, \quad \frac{\mathrm{d}\epsilon}{\mathrm{d}t'} = C_{\epsilon 1} P \frac{\epsilon}{k} - C_{\epsilon 2} \frac{\epsilon^2}{k}, \tag{1}$$

where k is the turbulent kinetic energy and is defined as $k = \frac{1}{2}\left(\langle u^2\rangle + \langle v^2\rangle + \langle w^2\rangle\right)$; ϵ is its dissipation; and $\langle u^2\rangle$, $\langle v^2\rangle$, and $\langle w^2\rangle$ are the velocity intensities in the streamwise, transverse, and spanwise directions, respectively, with $\langle\ \rangle$ denoting the ensemble average. In addition, t' [s] is the dimensional time, and P is the production term. Here, $t' = t'_r - t'_o$, where t'_r and t'_o are the actual time and the virtual origin of the time, respectively. $C_{\epsilon 1}$ and $C_{\epsilon 2}$ are model coefficients. The values of these model coefficients are $C_{\epsilon 1} = 1.44$ and $C_{\epsilon 2} = (n+1)/n$, where n is the decay exponent. The governing equations include the production term P because of the fluid acceleration caused by wind tunnel blockage. The production term is defined as $P = \frac{1}{2}\left(-2\langle u^2\rangle + \langle v^2\rangle + \langle w^2\rangle\right)(\mathrm{d}U/\mathrm{d}x)$, where $\mathrm{d}U/\mathrm{d}x$ is the longitudinal gradient of the streamwise mean velocity U and x is the streamwise direction. Introducing $a = \langle v^2\rangle/\langle u^2\rangle = \langle w^2\rangle/\langle u^2\rangle$ (e.g., Comte-Bellot and Corrsin, 1966) yields the following equation:

$$P = P_o \frac{\mathrm{d}U}{\mathrm{d}x} k(t'), \quad \text{where } P_o = \frac{2(a-1)}{1+2a}. \tag{2}$$

The expression $2(a-1)/(1+2a)$ can be considered to be constant when a is sufficiently constant (e.g., Comte-Bellot and Corrsin, 1966; Lavoie et al., 2007).

The turbulent kinetic energy in a homogeneous turbulence with no production term is given by the following power law:

$$k(t') = k_o \left(t'/t'_c\right)^{-n}, \tag{3}$$

where k_o is the decay coefficient of the turbulent kinetic energy and t'_c is the characteristic time of the bulk flow. For instance, when the formula for t'_c is derived by focusing on the grid-generated turbulence, t'_c is derived as $t'_c = M/U_o$, where U_o and M are the uniform inflow velocity and mesh size and are taken to be the characteristic velocity and length, respectively. The governing equations were analyzed by introducing the reference state, which is defined as the state in which

[DOI: 10.1299/jfst.2016jfst0012]

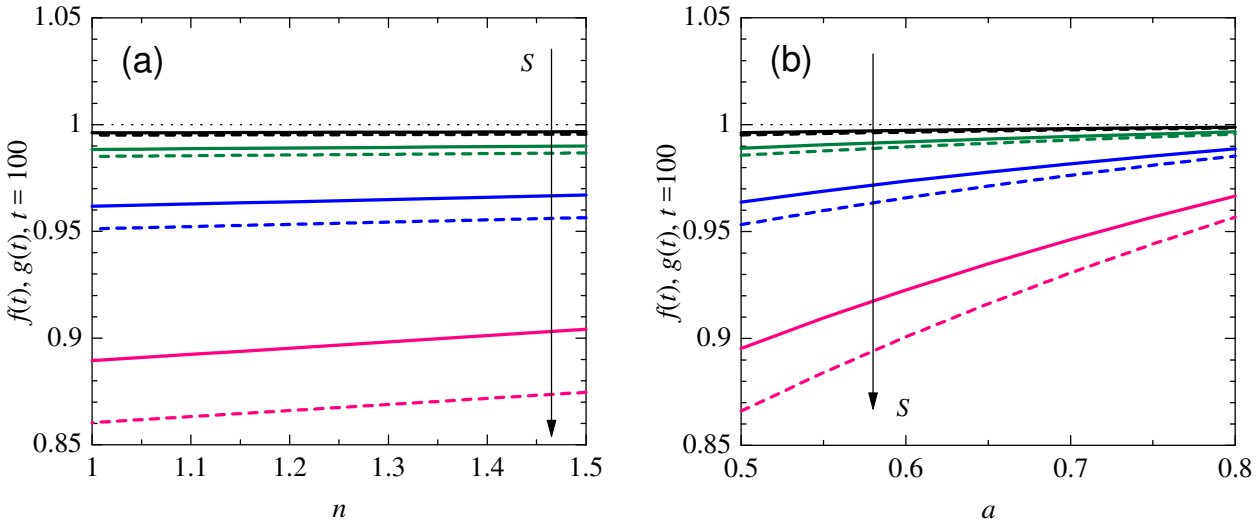

Fig. 2 Dependence of influence functions f and g at $t = 100$ on (a) n at $a = 0.5$ and (b) a at $n = 1.2$. Same key as in Fig. 1. The influence functions are more sensitive to changes in a than to changes in n.

the production term due to the acceleration is not present. To quantify the fluid acceleration effect, two nondimensional functions $f(t)$ and $g(t)$ were introduced as follows:

$$k(t) = f(t)\, k_o\, t^{-n},\ \epsilon(t) = g(t)\, \epsilon_o\, t^{-(n+1)},\ \text{where } \epsilon_o = \frac{nU_o}{M} k_o \text{ and } t = \frac{t'}{t'_c} = \frac{t'_r - t'_o}{t'_c}. \tag{4}$$

The influence functions $f(t)$ and $g(t)$ describe the effect of the fluid acceleration on the turbulent kinetic energy and its dissipation, respectively. Combining these two functions and the governing equations of the k–ϵ model yields

$$\begin{aligned} \frac{\mathrm{d}f}{\mathrm{d}t} &= P_o S\, f(t) + n\, \frac{f(t) - g(t)}{t} \\ \frac{\mathrm{d}g}{\mathrm{d}t} &= C_{\epsilon 1} P_o S\, g(t) + (n+1)\, \frac{g(t)}{f(t)}\, \frac{f(t) - g(t)}{t}, \end{aligned} \tag{5}$$

where $S = (\mathrm{d}U/\mathrm{d}x)/(U_o/M)$ is a nondimensional parameter that characterizes the magnitude of the fluid acceleration. Note that the derived governing equation does not include k_o or ϵ_o. This indicates that the solutions of the governing equation do not depend on these two quantities. Three parameters, P_o, S, and n, are included in the governing equation, meaning the effect of the fluid acceleration on the decaying homogeneous turbulence is governed by these three parameters.

2.2. Numerical results

First, the governing equations were numerically simulated. Following previous studies on grid-generated turbulence and turbulent boundary layers with zero pressure gradient, S was set to 1×10^{-4}, 3×10^{-4}, 1×10^{-3}, and 3×10^{-3}, and n was varied from 1 to 1.5. Again following previous studies on grid-generated turbulence (e.g., Comte-Bellot and Corrsin, 1966; Lavoie et al., 2007; Kurian and Frandson, 2009), a was varied from 0.5 to 0.8. A fourth-order Runge–Kutta scheme was used to integrate the numerical results. The governing equations were analyzed up to $t = 100$, with $f(0) = g(0) = 1$, which indicates that there was no fluid acceleration effect in the initial state. Figure 1 shows the temporal variation of the influence functions $f(t)$ and $g(t)$ at $a = 0.5$ and $n = 1.2$. The fluid acceleration caused the magnitude of the turbulent kinetic energy and its dissipation to decrease over time. These results agree qualitatively with those of previous experiments (e.g., Kurian and Frandson, 2009). The effect of the fluid acceleration increased as S increased. The dissipation is more sensitive than the turbulent kinetic energy to the acceleration effect. Although the shape of the evolutions is nearly linear, the deviation of the red dashed line representing $g(t)$ from the thin dashed line representing a linear function with a slope equal to the initial gradient of $g(t)$ indicates that the influence functions are not linear.

Figure 2 shows the effect of the parameters n and a of the governing equations on the influence functions f and g at $t = 100$. Figure 2(a) shows the effect of n on $f(100)$ and $g(100)$ at $a = 0.5$. Although the influence functions were affected by changing n and increased as n decreased, they were more sensitive to changes in S. The effect of n on the influence functions decreased as their magnitudes decreased. Figure 2(b) shows the effect of a on $f(100)$ and $g(100)$ at $n = 1.2$. The

[DOI: 10.1299/jfst.2016jfst0012]

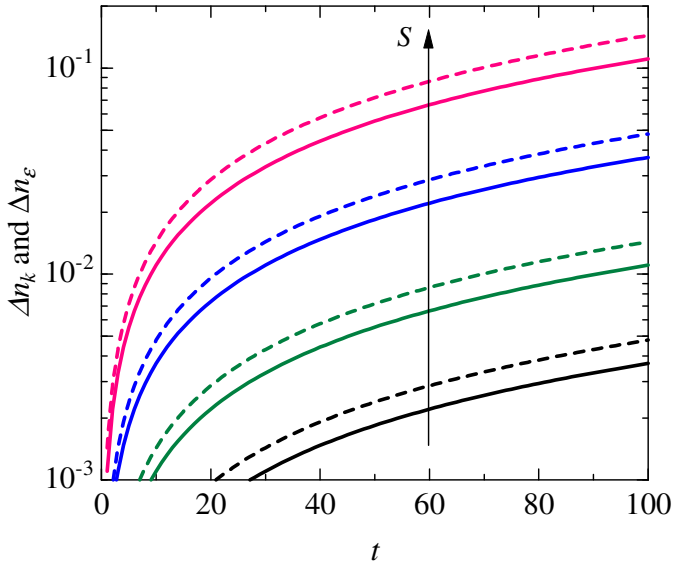

Fig. 3 Temporal evolution of Δn_k and Δn_ϵ. The solid black and dashed red lines represent the results of Δn_k and Δn_ϵ, respectively. The deviations Δn_k and Δn_ϵ increased with increasing S and reached values on the order of 0.1. Therefore, large values of S have a non-negligible effect on the decay exponents.

observed effect of the fluid acceleration decreased as a increased. The rates of change of $f(t)$ and $g(t)$ with respect to a decreased as the magnitudes of $f(t)$ and $g(t)$ decreased. These results indicate that the acceleration effect is more sensitive to a than to n.

The decay exponent characterizes the decaying homogeneous turbulence. An accurately measured value of the decay exponent should be used when examining the characteristics of the decaying homogeneous turbulence. This section describes the effect of the fluid acceleration on the decay exponent. When there is no fluid acceleration effect, the decay exponents of the turbulent kinetic energy and the dissipation are calculated as

$$n = -\frac{t\,\mathrm{d}k/\mathrm{d}t}{k(t)}, n+1 = -\frac{t\,\mathrm{d}\epsilon/\mathrm{d}t}{\epsilon(t)}. \tag{6}$$

The effect of the fluid acceleration on the decay exponents was investigated using the analytical solutions of f and g as

$$\begin{aligned} n_k &= n + \Delta n_k = -\frac{t\,\mathrm{d}k/\mathrm{d}t}{k(t)},\ \Delta n_k = -\frac{t\,\mathrm{d}f/\mathrm{d}t}{f(t)} \text{ and} \\ n_\epsilon + 1 &= n + 1 + \Delta n_\epsilon = -\frac{t\,\mathrm{d}\epsilon/\mathrm{d}t}{\epsilon(t)},\ \Delta n_\epsilon = -\frac{t\,\mathrm{d}g/\mathrm{d}t}{g(t)}, \end{aligned} \tag{7}$$

where n_k and $n_\epsilon + 1$ are the observed decay exponents for k and ϵ, respectively, when the fluid acceleration effect is present and Δn_k and Δn_ϵ are the deviations of the decay exponents for k and ϵ, respectively, due to the fluid acceleration. Figure 3 shows the temporal evolution of Δn_k and Δn_ϵ. Both deviations increased over time and with increasing S. In all cases, Δn_ϵ was larger than Δn_k. The shapes of the profiles were also similar among the different values of S.

The results of the numerical simulation can be summarized as follows. The fluid acceleration affects both the turbulent kinetic energy and its dissipation. The dissipation is more sensitive than the energy to the fluid acceleration. The fluid acceleration effect was more sensitive to changes in a than to changes in n. The fluid acceleration affects the decay exponent of the decaying turbulence. When S is large, the deviation in the decay exponent caused by the fluid acceleration is non-negligible.

3. Validation scheme

3.1. Derivation

Formulas for $f(t)$ and $g(t)$ were obtained to produce a validation scheme. The expression $(f(t) - g(t))/t$ was used to derive these functions from the governing equations. Analytical solutions for $f(t)$ and $g(t)$ were derived by modeling the expression $(f(t) - g(t))/t$. Figure 4 shows the temporal variation of $(f(t) - g(t))/t$. The magnitude of $(f(t) - g(t))/t$ depends on that of S. When the magnitude of S is decreased, $(f(t) - g(t))/t$ decreases. The magnitude of $(f(t) - g(t))/t$ is nearly constant with respect to time. The dotted lines in the figure represent the following approximation, which was

[DOI: 10.1299/jfst.2016jfst0012]

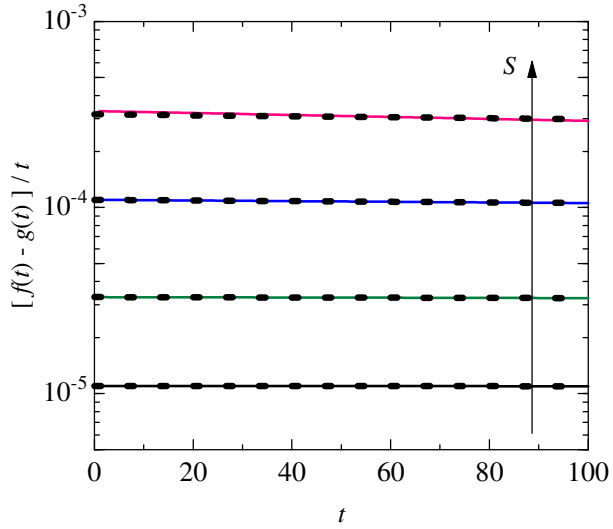

Fig. 4 Temporal variation of $(f(t) - g(t))/t$. The solid black, green, blue, and red lines represent the results at $S = 1 \times 10^{-4}$, 3×10^{-4}, 1×10^{-3}, and 3×10^{-3}, respectively. The dotted lines indicate the fit of Eq. (8) to $(f(t) - g(t))/t$ at each value of S. The temporal variation $(f(t) - g(t))/t$ can be approximated by Eq. (8) and is nearly constant when S is small.

fitted to each distribution:

$$\frac{f(t) - g(t)}{t} = h, \quad \text{where } h = C_1. \tag{8}$$

The equation $(f(t) - g(t))/t = h$ fitted to the results agrees well with each distribution of $(f(t) - g(t))/t$. This agreement indicates that the above equation approximates $(f(t) - g(t))/t$ with sufficient accuracy.

By introducing this approximation, analytical solutions of $f(t)$ and $g(t)$ can be derived from the governing equation of $f(t)$.The following form of the constant distribution of h was assumed based on the results shown in Fig. 4:

$$h = C_1 = CP_oS, \tag{9}$$

where C is a constant. Using the assumed form of the constant h, the governing equation of $f(t)$ takes the form of a linear first-order ordinary differential equation, which can be solved analytically. The analytical solutions of $f(t)$ and $g(t)$ are

$$\begin{aligned} f(t) &= (1 + Cn)\, e^{P_oSt} - Cn \\ g(t) &= (1 + Cn)\, e^{P_oSt} - C(n + P_oSt), \end{aligned} \tag{10}$$

where the solution of $g(t)$ was derived from $h = CP_oS$ and $f = g = 1$ in the initial state.

The relationship between the constant C in the approximation of $(f(t) - g(t))/t$ and the constant $C_{\epsilon 1}$ in the governing equations was derived. The derived solutions of $f(t)$ and $g(t)$ given by Eq. (10) include the approximation coefficient C. The equation for C was derived using the governing equation of $g(t)$ (Eq. (5)). When S is small, the two sides of the governing equation of $g(t)$ can be approximated as

$$\begin{aligned} \text{(LHS)} &= (1 + Cn - C)\, P_oS + \cdots \\ \text{(RHS)} &= (C_{\epsilon 1} + Cn + C)\, P_oS + \cdots, \end{aligned} \tag{11}$$

where (LHS) and (RHS) refer to the left- and right-hand sides of the governing equation of $g(t)$ (Eq. (5)), respectively. Equating the two expressions yields the following simple equation relating C and $C_{\epsilon 1}$ and a new form for h:

$$C = -\frac{C_{\epsilon 1} - 1}{2}, \qquad h = CP_oS = -\frac{C_{\epsilon 1} - 1}{2} P_oS. \tag{12}$$

The coefficient C is a function of only $C_{\epsilon 1}$.

The derived equations of $f(t)$ and $g(t)$ were then validated. First, the model $(f(t) - g(t))/t = h$ was validated. Figure 5(a) validates this model by Eq. (12). The value of this model was found to agree well with the numerical results, validating the models of C and the constant h. Substituting Eq. (12) into Eq. (10) yields the following analytical solutions

[DOI: 10.1299/jfst.2016jfst0012]

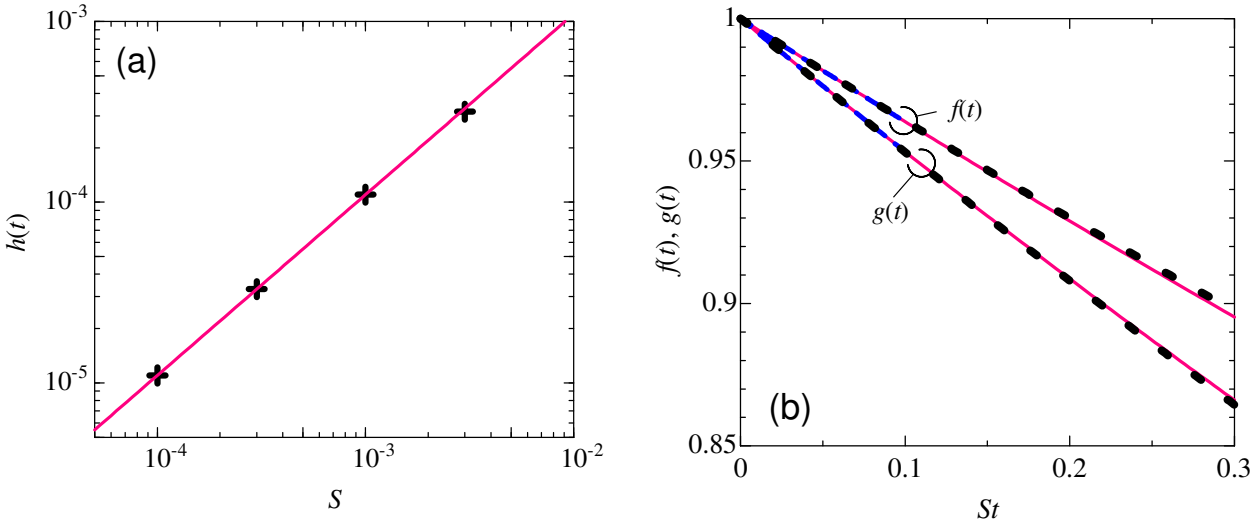

Fig. 5 Validation of fluid acceleration effect formulas. (a) Validation of the model $(f(t) - g(t))/t = h$, where h was measured to be C_1. The symbols indicate the numerical results for h. The red line represents $h = -\frac{1}{2}(C_{\epsilon 1} - 1)P_o S$. The agreement between the numerical results and this formula validates the derived equation of the coefficient (Eq. (12)). (b) Validation of influence functions $f(t)$ and $g(t)$, which predict the fluid acceleration effect. The solid red and dashed blue lines represent the numerical results for $S = 3{\times}10^{-3}$ and 1×10^{-3}, respectively. The dotted black lines indicate the results of the validation scheme (Eq. (13)). The agreement between the numerical and algebraic results for $f(t)$ and $g(t)$ validates the approximation of $f(t)$ and $g(t)$ given by the validation scheme.

of $f(t)$ and $g(t)$:

$$f(t) = e^{P_o S t} - \frac{n}{2}(C_{\epsilon 1} - 1)\left(e^{P_o S t} - 1\right)$$
$$g(t) = e^{P_o S t} - \frac{n}{2}(C_{\epsilon 1} - 1)\left(e^{P_o S t} - 1 - \frac{P_o S}{n}t\right). \tag{13}$$

Figure 5(b) validates the solutions of $f(t)$ and $g(t)$ at $S = 3 \times 10^{-3}$ and 1×10^{-3}, with the governing equations integrated up to $t = 100$. When plotted against St, both variations converged. The analytical solutions of $f(t)$ and $g(t)$ were found to agree well with the numerical simulation results. This agreement validates the derived solutions of $f(t)$ and $g(t)$. When St exceeded 0.2, the derived solutions deviated slightly from the numerical results, indicating that the derived solutions are accurate for small St.

3.2. Discussion

The analytical solutions of $f(t)$ and $g(t)$ given earlier were derived using the model $h(t) = -(1/2)(C_{\epsilon 1} - 1)P_o S$. The physical meaning of the model is discussed in this section. Using the rates of change of $f(t)$ and $g(t)$ at $t = 0$, $f(t)$ and $g(t)$ can be approximated as

$$f(t) = 1 + t\left.\frac{\mathrm{d}f}{\mathrm{d}t}\right|_{t=0}, g(t) = 1 + t\left.\frac{\mathrm{d}g}{\mathrm{d}t}\right|_{t=0}, \tag{14}$$

where $f(0) = g(0) = 1$. Based on these approximations, the relation $h = -(1/2)(C_{\epsilon 1} - 1)P_o S$ yields

$$h = \left.\frac{\mathrm{d}f}{\mathrm{d}t}\right|_{t=0} - \left.\frac{\mathrm{d}g}{\mathrm{d}t}\right|_{t=0} = -\frac{C_{\epsilon 1} - 1}{2}P_o S. \tag{15}$$

This relation clarifies the physical meaning of $h = -(1/2)(C_{\epsilon 1} - 1)P_o S$. The value $-(1/2)(C_{\epsilon 1} - 1)P_o S$ at $t = 0$ is equivalent to the difference between the rates of change of $f(t)$ and $g(t)$ at $t = 0$, which means this difference is proportional to P_o and S. The constant variation of the difference between the quantities was used to derive a simplified version of the analytical solution. Based on the solutions of $f(t)$ and $g(t)$, their initial rates of change were derived as

$$\left.\frac{\mathrm{d}f}{\mathrm{d}t}\right|_{t=0} = \left(1 - \frac{C_{\epsilon 1} - 1}{2}n\right)P_o S, \left.\frac{\mathrm{d}g}{\mathrm{d}t}\right|_{t=0} = \left(1 - \frac{C_{\epsilon 1} - 1}{2}n\right)P_o S + \frac{C_{\epsilon 1} - 1}{2}P_o S. \tag{16}$$

The equations describing the initial rates of change of the influence functions include the decay exponent. Although these rates of change depend on the decay exponent, their difference is independent of it.

[DOI: 10.1299/jfst.2016jfst0012]

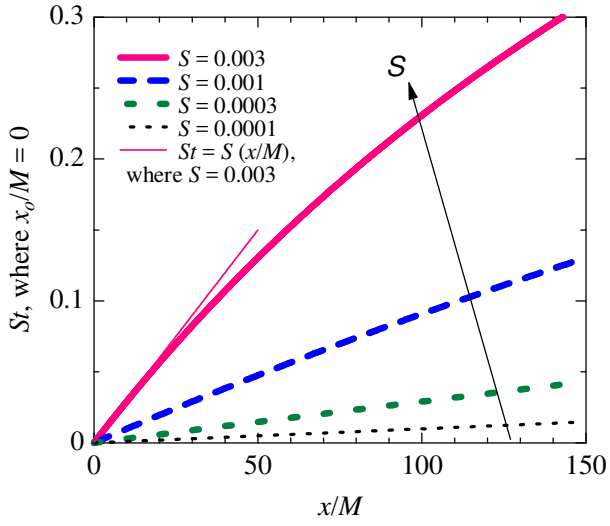

Fig. 6 St calculated from Eq. (18) with $x_o/M = 0$ ($St = (S(x/M))/(1 + S(x/M))$) plotted against x/M. The profile of St depends on the value of S.

Figure 5(b) shows the validation of the validation scheme. As shown in Fig. 5(b), the validation scheme was found to be accurate in the range of $St = 0 - 0.2$. Therefore, the application limit $(St)_l$ of this proposed scheme was estimated to be $(St)_l = 0.2$. In this study, the nondimensional time t was used. The nondimensional time t results in the following:

$$\begin{aligned} t = \frac{t'_r - t'_o}{t'_c} = \frac{t'_r - t'_o}{M/U_o} &= \frac{U_o}{U(x)}\frac{x}{M} - \frac{U_o}{U(x_o)}\frac{x_o}{M}, \\ &= \frac{U_o}{U_o + (\mathrm{d}U/\mathrm{d}x)\,x}\frac{x}{M} - \frac{U_o}{U_o + (\mathrm{d}U/\mathrm{d}x)\,x_o}\frac{x_o}{M} + \cdots \\ &= \frac{1}{1 + S(x/M)}\frac{x}{M} - \frac{1}{1 + S(x_o/M)}\frac{x_o}{M} + \cdots, \text{ where } x = U(x)t'_r \text{ and } x_o = U(x_o)t'_o. \end{aligned} \quad (17)$$

Here, the following linear approximation of U was used: $U = U_o + (\mathrm{d}U/\mathrm{d}x)\,x + \cdots$. Based on the above equation, St can be approximated as

$$St = \frac{S}{1 + S(x/M)}\frac{x}{M} - \frac{S}{1 + S(x_o/M)}\frac{x_o}{M}. \quad (18)$$

Figure 6 shows St plotted against x/M with $x_o/M = 0$. As shown in the figure, the approximation of St depends on the value of S; specifically, the rate of increase of St is large when S is large. For instance, as shown in Fig. 6, $\mathrm{d}(St)/\mathrm{d}(x/M)$ at $x/M = 0$ is given by $\mathrm{d}(St)/\mathrm{d}(x/M)|_{x/M=0} = (S/(1 + S(x/M)))|_{x/M=0} = S$. The upper limit of St can be set by defining the x/M limit $(x/M)_l$ with the use of Eq. (18). Equation (18) yields the following equation for the limit of S:

$$St = S\left(\frac{x}{M} - \frac{x_o}{M}\right) + \cdots \quad \text{therefore} \quad S_l = \frac{(St)_l}{(x/M)_l - (x_o/M)}, \quad (19)$$

where S_l is the limit of S and S is small. Setting the values of $(x/M)_l$ and (x_o/M) allows the limit S_l of S to be calculated. For instance, when $(x/M)_l = 200$ and $(x_o/M) = 0$, the limit of S is $S_l = 0.001$.

The uncertainty of the model coefficient produces uncertainty in $f(t)$ and $g(t)$ because the solutions of $f(t)$ and $g(t)$ include the model coefficient. Using the derived solutions, the effect of the uncertainty of the model coefficient on $f(t)$ and $g(t)$ was examined. To examine the effect of the uncertainty, the solutions of $f(t)$ and $g(t)$ were expanded at $C_{\epsilon 1} = C^o_{\epsilon 1}$. This yields the following approximations:

$$\begin{aligned} f(t) &= e^{P_o St} - \frac{n}{2}\left(C^o_{\epsilon 1} - 1\right)\left(e^{P_o St} - 1\right) - \frac{n}{2}(C_{\epsilon 1} - C^o_{\epsilon 1})P_o St + \cdots \\ g(t) &= e^{P_o St} - \frac{n}{2}\left(C^o_{\epsilon 1} - 1\right)\left(e^{P_o St} - 1 - \frac{P_o S}{n}t\right) - \frac{n-1}{2}(C_{\epsilon 1} - C^o_{\epsilon 1})P_o St + \cdots. \end{aligned} \quad (20)$$

The third terms on the right-hand sides of Eq. (20) represent the effects of the uncertainty of the model coefficient on $f(t)$ and $g(t)$. These terms are linear approximations of the original forms, which are based on an exponential function. The linear approximations were derived under the assumption that S has a small magnitude. The effect of the uncertainty of the model coefficient on $f(t)$ and $g(t)$ depends on the decay exponent, as demonstrated by Eq. (20). The coefficients n

[DOI: 10.1299/jfst.2016jfst0012]

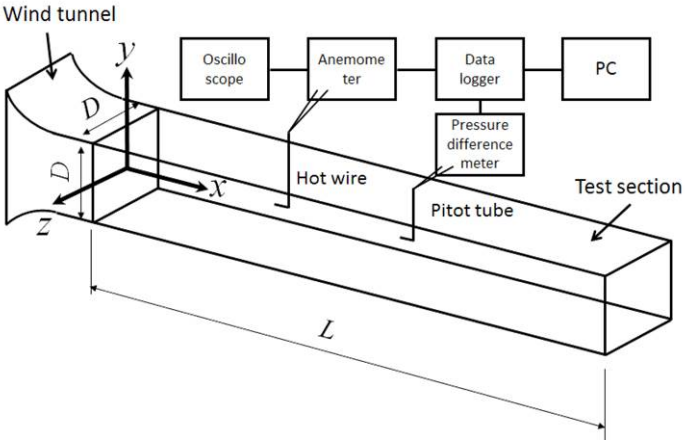

Fig. 7 Schematic of the experimental apparatus. The present experimental apparatus consists of a wind tunnel with an entrance area of $D^2 = (200\,\mathrm{mm})^2 = 400\,\mathrm{cm}^2$, and a measurement system, the primary components of which are a standard JIS-type pitot tube, a constant temperature anemometer, and a differential manometer. The observed values of the free stream velocity are approximately 14 and 18 m/s.

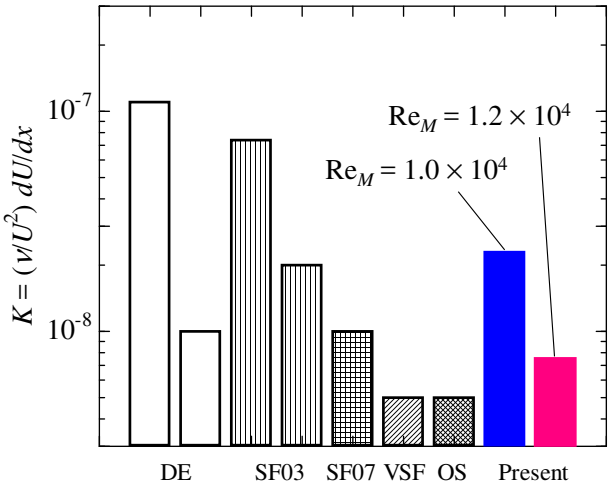

Fig. 8 Values of K obtained in previous experiments and the present study. DE, SF03, SF07, VSF, and OS indicate results obtained by de Graaff and Eaton (2000), Schultz and Flack (2003), Schultz and Flack (2007), Volino et al. (2009, 2011), and Örlü and Schlatter (2013), respectively. The blue and red vertical bars show the results of the present experiment. K shown by the blue bars is larger than that by the red bar. The values of K obtained in the present study are comparable to those obtained in previous experiments on turbulent boundary layers with zero pressure gradient.

and $(n-1)$ represent the magnitudes of the effect of the uncertainty of the model coefficient on $f(t)$ and $g(t)$, respectively. The value of n is on the order of unity. Because $(n-1)$ is less than n, the uncertainty of the model coefficient has less of an impact on the effect of the acceleration on the dissipation than on that of the turbulent kinetic energy. Previous studies have indicated that the decay exponent increases with decreasing Reynolds number (e.g., Kurian and Fransson, 2009). Therefore, the effect of the uncertainty on the dissipation influence function increases as the Reynolds number decreases. The value of $|g(t)-1|$ is larger than that of $|f(t)-1|$, as shown in the previous figure. Therefore, the dissipation is more sensitive than the turbulent kinetic energy to the fluid acceleration. The effect of the fluid acceleration on the dissipation is less sensitive than that on the turbulent kinetic energy to the uncertainty of the model coefficient. Therefore, focusing on the effect of the fluid acceleration on the dissipation reduces the effect of the uncertainty of the model coefficient.

A decaying homogeneous turbulence is fundamentally characterized by its decay exponent. An accurately measured value of the decay exponent should be used when examining the characteristics of a decaying homogeneous turbulence. Deviations in the decay exponent due to the fluid acceleration can be obtained from $f(t)$ and $g(t)$ (Eq. (7)). The deviations Δn_k and Δn_ϵ in the decay exponents for k and ϵ due to the fluid acceleration can be described using the analytical solutions of $f(t)$ and $g(t)$ (Eq. (13)). The original equations for the deviations in the decay exponents (Eq. (7)) derived from the analytical solutions are not appropriate because of the complexity of the analytical solutions. When the value of S is

[DOI: 10.1299/jfst.2016jfst0012]

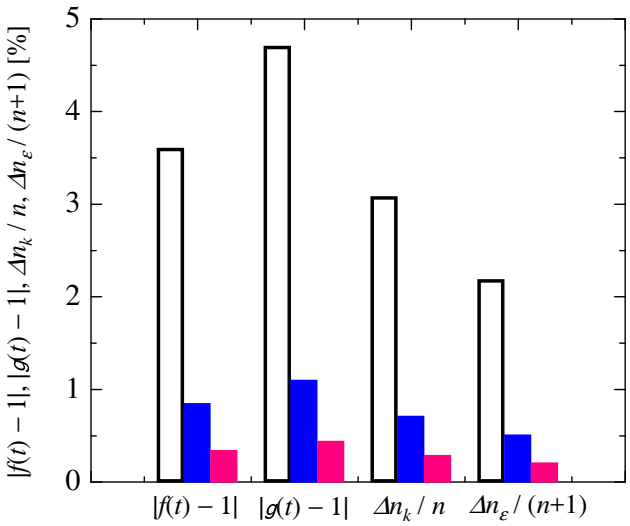

Fig. 9 Effect of fluid acceleration on the following quantities characterizing the decaying turbulence: $|f(t)-1|$, $|g(t)-1|$, $\Delta n_k/n$, and $\Delta n_\epsilon/(n+1)$. The blue and red vertical bars show the results for $\mathrm{Re}_M = 1.0\times10^4$ and 1.2×10^4, respectively. The open bars show the results for $S = 1\times10^{-3}$. The quantities are given as percentages. Although the acceleration effect at $S = 1\times10^{-3}$ is relatively large, the effect at the present value of S is considered to be small.

small, the deviations in the decay exponents can be approximated as

$$\Delta n_k = -\frac{t\,\mathrm{d}f/\mathrm{d}t}{f(t)} = \frac{(C_{\epsilon1}-1)\,n-2}{2}P_o S\,t+\cdots$$
$$\Delta n_\epsilon = -\frac{t\,\mathrm{d}g/\mathrm{d}t}{g(t)} = \frac{(C_{\epsilon1}-1)\,n-C_{\epsilon1}-1}{2}P_o S\,t+\cdots. \tag{21}$$

The accuracy of these approximations was then examined. At $S = 1\times10^{-3}$, $P_o = -1/2$, and $t = 100$, the original equations (Eq. (7)) and the approximations (Eq. (21)) yielded values of 0.0363... and 0.0368 for Δn_k, and 0.0483... and 0.0478 for Δn_ϵ, respectively. In actual experiments, the decay exponent can be calculated to two decimal places. Therefore, these linear approximations are considered to be sufficiently accurate for actual experiments.

George and Wang (2009) discussed the decay of homogeneous turbulence from a perspective different from that of the present study. They considered a type of homogeneous turbulence in which the decay of the kinetic energy follows an exponential function. This exponential decay is caused by the constant nature of the length scales. A similar point of view can be found in a study by Wang and George (2002), which discusses the effects of the nature of the integral length scale on the decay of homogeneous turbulence. These previous studies consider the production terms arising from the fluid acceleration. In contrast to these studies, the present study considered the effect of a small acceleration on the decay of a homogeneous turbulence. The difference between the present study and the abovementioned previous studies is the consideration of the production terms.

4. Experiment on grid-generated turbulence

4.1. Experimental methods

The validation scheme (Eq. (13)) was used to experimentally examine the effect of fluid acceleration due to wind tunnel blockage. Figure 7 shows a schematic of the wind tunnel. The streamwise, transverse, and spanwise directions are represented by x, y, and z, respectively. The origin of the coordinate system is located at the center of the cross-sectional area at the entrance. The length of the test section in the streamwise direction is 2410 mm. The cross-sectional area D^2 at the entrance is $(200\,\mathrm{mm})^2 = 400\,\mathrm{cm}^2$. The test section is made of acrylic resin. A traverse system was placed above the test section, and a diffuser was placed at the end of the test section. The relative root mean square (RMS) of the background flow was approximately $0.2\% - 0.3\%$. Boundary layers formed on the side walls. The effective area of the tunnel cross section decreased with increasing x because of the development of the boundary layers. The decreasing effective cross-sectional area resulted in fluid acceleration due to wind tunnel blockage. The tunnel was expanded in the spanwise direction to reduce the fluid acceleration. The rate of this expansion was several hundredths of a percent per meter. A turbulence-generating grid was placed at the entrance. This grid is biplanar and consists of round rods with a diameter d of 2 mm. The mesh size M is 10 mm, meaning the solidity σ is 0.36. The resulting value of $D/M = 20$ was

[DOI: 10.1299/jfst.2016jfst0012]

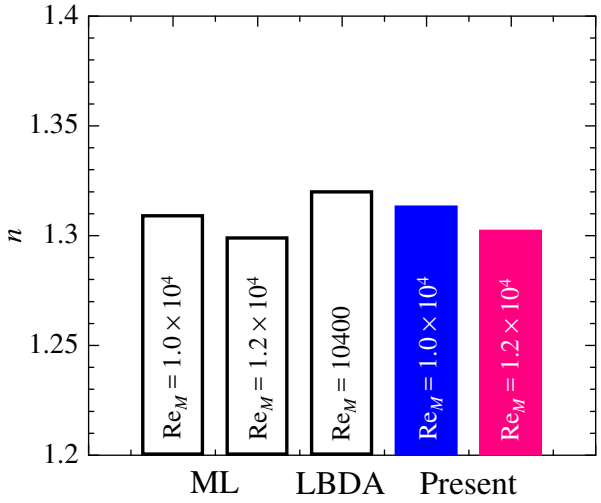

Fig. 10 Decay exponent of grid-generated turbulence. ML and LBDA indicate the results obtained by Mohamed and LaRue (1990) and Lavoie et al. (2005), respectively. The specifications of the turbulence-generating grid of the three experiments are listed in Table 1. The virtual origin of the present profiles was set to zero, as in the previous experiments. The decay exponent values obtained in the present experiment agree with those obtained in the previous experiments.

Table 1 Geometry and conditions of grid-generated turbulence in the present experiment and previous studies. The shape of the present turbulence-generating grid is similar to those used in the previous experiments.

Study	Re_M	bar shape	σ	x_o/M
Present	$1.0\times10^4, 1.2\times10^4$	round rod	0.36	0
Mohamed and LaRue (1990)	$1.0\times10^4, 1.2\times10^4$	round rod	0.34	0
Lavoie et al. (2005)	1.04×10^4	round rod	0.35	0

considered to be sufficient. The Reynolds number based on the mesh size, which is defined as $\mathrm{Re}_M = U_o M/\nu$, was set to approximately 1.0×10^4 or 1.2×10^4. U_o was approximately 14 and 18 m/s for the lower and higher Reynolds numbers, respectively.

In this experiment, the streamwise mean velocity U and streamwise velocity fluctuation u were measured. The streamwise mean velocity was measured using a standard JIS-type pitot tube, the coefficient of which was accurately calibrated. The coefficient is weakly dependent on the Reynolds number and has a small uncertainty, and its mean value was 0.9985 ± 0.0005. The static pressure was measured using a differential manometer (SIBATA, ISP-750). By calibrating the differential manometer before all sets of measurements, the effect of the ambient temperature variation on the measurement results was reduced. The effect of free-stream turbulence on the observed mean velocity was smaller than the uncertainty of the coefficient. Constant temperature anemometry (CTA) was used to measure the velocity fluctuation along the center line. CTA (SOKKEN, HC-30) was conducted using I-type hot wire made in house. The hot wire was a tungsten wire with a diameter of 5 μm. The aspect ratio was approximately 200. The relative difference between the calibration curves obtained before and after calibration was sufficiently small. The differential manometer was calibrated before each CTA measurement calibration. Measured analog data from the CTA was sampled by a data logger (KEYENCE, NR-600) with 14-bit depth. The sampling frequency and sampling time were 20 kHz and 60 s, respectively. A personal computer (PC) was used to process the observed digital data. The uniformity of the grid-generated turbulence was confirmed in the measurement range using the mean velocity and the RMS, skewness, and flatness factors of the velocity fluctuation.

4.2. Results

The acceleration parameter was measured. In previous experiments in which boundary layer flows were measured, the fluid acceleration effect was quantified by the acceleration parameter $K = (\nu/U^2)(\mathrm{d}U/\mathrm{d}x)$ (de Graaff and Eaton, 2000). Another definition based on the streamwise pressure gradient has also been used in previous experiments (e.g., Osaka et al., 1998; Örlü and Schlatter, 2013). This definition requires the acceleration parameter to be sufficiently small in an observed turbulent boundary layer with zero pressure gradient. In the present experiment, the following equation was fitted to the measurement results for the gradient of the streamwise mean velocity: $U = U_o + (\mathrm{d}U/\mathrm{d}x)x$. The mean velocity at each position may deviate slightly from the fitted equation. The relative RMS of the mean velocity was approximately

[DOI: 10.1299/jfst.2016jfst0012]

0.4%. Based on the measurement results, the acceleration parameters at $\mathrm{Re}_M = 1.0 \times 10^4$ and 1.2×10^4 were calculated to be $K = 2.3 \times 10^{-8}$ and 7.5×10^{-9}, respectively.

Figure 8 shows the acceleration parameter values obtained in the present study and in previous experiments in which zero-pressure gradient turbulent boundary layers were measured. The range of acceleration parameter values is rather large. The maximum value in the previous experiments was approximately 1×10^{-7}. The present values of K are comparable with those obtained in previous experiments on obtaining the zero-pressure gradient turbulent boundary layer.

Using the equations derived for $f(t)$ and $g(t)$, the fluid acceleration effect in the present wind tunnel was quantified and is considered to be small. The values of S at $\mathrm{Re}_M = 1.0 \times 10^4$ and 1.2×10^4 were calculated to be $S = 2.3 \times 10^{-4}$ and 9.0×10^{-5}, respectively. S was also set to $S = 1.0 \times 10^{-3}$, which corresponds to $K = 1.0 \times 10^{-7}$ at approximately $\mathrm{Re}_M = 1.0 \times 10^4$. The following values were also set: $t = 100$, $C_{\epsilon 1} = 1.44$, and $n = 1.2$. The previously derived equations were used to calculate $f(t)$, $g(t)$, and the deviations of the decay exponents. The values of the influence functions and deviations under the abovementioned conditions are summarized in Fig. 9. The absolute values of the relative deviations of $f(t) - 1$ and $g(t) - 1$ were smaller than 1.5%. The absolute relative values of the deviation of the decay exponents were also smaller than 1%. These results validate the moderate-sized wind tunnel examined in the present study, in which the fluid acceleration effect is negligible.

The decay characteristics of the present grid-generated turbulence in the validated wind tunnel were investigated. Table 1 compares the geometry and conditions of the present grid-generated turbulence with those of previous experiments (Mohamed and LaRue, 1990; Lavoie et al., 2005). Table 1 indicates that the geometry and conditions of the previous experiments are similar to those of the present grid-generated turbulence. Figure 10 shows the decay exponent of the streamwise velocity fluctuation intensity obtained in the present experiment. The virtual origin of the profiles was set to zero. Figure 10 also demonstrates that the profiles of the intensity were well approximated by each power law with sufficient accuracy. The values of the decay exponent obtained in the present study were found to agree with those obtained in the previous experiments.

5. Conclusion

The decay exponent characterizes decaying grid-generated turbulence generated in a wind tunnel. The development of boundary layers on the side walls of wind tunnels reduces the effective cross-sectional area of the wind tunnel, resulting in fluid acceleration, which affects the turbulent kinetic energy. The fluid acceleration effect is more significant in wind tunnels with smaller cross-sectional areas. The magnitude of the fluid acceleration should be sufficiently small because the decay characteristics are affected by the fluid acceleration.

In the present study, a validation scheme for the fluid acceleration effect on the characteristics of the decaying turbulence was developed. This scheme was derived from the k–ϵ model of homogeneous turbulence. The modified governing equations of the fluid acceleration effect on the turbulent kinetic energy and the dissipation were then derived. Based on the numerical results obtained using the modified equations, a term in the governing equations was modeled. Using this model, the analytical solutions of the effect of the fluid acceleration on the turbulent kinetic energy and its dissipation were derived. These influence functions were then validated through numerical simulation. In addition, equations describing the effect of the fluid acceleration on the decay exponents were derived. The dissipation was found to be more sensitive than the turbulent kinetic energy to the fluid acceleration. The effect of the uncertainty of the model coefficient on the influence functions was also examined. The effect of the fluid acceleration on the dissipation was less sensitive than that on the turbulent kinetic energy to the uncertainty of the model coefficient. Using the validation scheme, a moderate-sized wind tunnel in which the fluid acceleration is reduced was validated. The effect of the fluid acceleration on the turbulent kinetic energy and its dissipation in the wind tunnel was calculated using the validation scheme and was found to be sufficiently small. The decay exponent of the grid-generated turbulence in the wind tunnel was then determined. The values of the decay exponent obtained in this study agree with those obtained in previous experiments.

The validation scheme of the fluid acceleration effect derived in the present study will be helpful to quantify discussions of the decay characteristics of grid-generated turbulence. The presented equations quantifying the acceleration effect could be used to separate the effects of the uncertainty of the measurement and that of the generated turbulence. The validation scheme could also be applied to the correction of the effect of acceleration due to wind tunnel blockage.

Acknowledgments

The authors would like to thank Dr. Tatsuo Ushijima (Nagoya Institute of Technology) for his fruitful discussion and Mr. Shinnosuke Matsuo (Nagoya Institute of Technology) for his assistance in conducting the experiment. The present study was supported in part by the Japanese Ministry of Education, Culture, Sports, Science and Technology through Grants-in-Aid (Nos. 25289030, 25420115, 15K05792, 15K13871, and 15K17970).

[DOI: 10.1299/jfst.2016jfst0012]

References

Barlow, J. B., Rae, W. H. and Pope, A. Low-Speed Wind Tunnel Testing (1999), pp.665-679, Wiley-Interscience.

Bennett, J. C. and Corrsin, S., Small Reynolds number nearly isotropic turbulence in a straight duct and a contraction, Physics of Fluids, Vol.21, No.12 (1978), pp.2129-2140.

Comte-Bellot, G. and Corrsin, S., The use of a contraction to improve the isotropy of grid-generated turbulence, Journal of Fluid Mechanics, Vol.25, No.4 (1966), pp.657-682.

Davidson, P. A., The minimum energy decay rate in quasi-isotropic grid turbulence, Physics of Fluids, Vol.23, No.8 (2011), 085108.

De Graaff, D. B. and Eaton, J. K., Reynolds-number scaling of the flat-plate turbulent boundary layer, Journal of Fluid Mechanics, Vol.422, No.1 (2000), pp.319-346.

George, W. K., The decay of homogeneous isotropic turbulence, Physics of Fluids A, Vol.4, No.7 (1992), pp.1492-1509.

George, W. K. and Wang, H., The exponential decay of homogeneous turbulence, Physics of Fluids, Vol.21, No.2 (2009), 025108.

Hinze, J. O., Turbulence (1975), pp.268-269, Mcgraw-Hill.

Krogstad, P. Å. and Davidson, P. A., Is grid turbulence Saffman turbulence ?, Journal of Fluid Mechanics, Vol.642 (2010), pp.373-394.

Kurian, T. and Fransson, J. H., Grid-generated turbulence revisited, Fluid Dynamics Research, Vol.41, No.2 (2009), 021403.

Lavoie, P., Burattini, P., Djenidi, L. and Antonia, R. A., Effect of initial conditions on decaying grid turbulence at low R_λ, Experiments in fluids, Vol.39, No.5 (2005), pp.865-874.

Lavoie, P., Djenidi, L. and Antonia, R. A., Effects of initial conditions in decaying turbulence generated by passive grids, Journal of Fluid Mechanics, Vol.585 (2007), pp.395-420.

Meldi, M. and Sagaut, P., On non-self-similar regimes in homogeneous isotropic turbulence decay, Journal of Fluid Mechanics, Vol.711 (2012), pp.364-393.

Mohamed, M. S. and LaRue, J. C., The decay power law in grid-generated turbulence, Journal of Fluid Mechanics, Vol.219 (1990), pp.195-214.

Nagata, K., Sakai, Y., Inaba, T., Suzuki, H., Terashima, O. and Suzuki, H., Turbulence structure and turbulence kinetic energy transport in multiscale/fractal-generated turbulence, Physics of Fluids, Vol.25 (2013), 065102.

Örlü, R. and Schlatter, P., Comparison of experiments and simulations for zero pressure gradient turbulent boundary layers at moderate Reynolds numbers, Experiments in fluids, Vol.54, No.6 (2013), pp.1-21.

Osaka, H., Kameda, T. and Mochizuki, S., Re-examination of the Reynolds-number-effect on the mean flow quantities in a smooth wall turbulent boundary layer, JSME International Journal Series B, Vol.41, No.1 (1998), pp.123-129.

Pope, S. B., Turbulent Flows (2000), pp.158-160 and pp.373-378, Cambridge University Press.

Schultz, M. P. and Flack, K. A., Turbulent boundary layers over surfaces smoothed by sanding, Journal of Fluids Engineering, Vol.125, No.5 (2003), pp.863-870.

Schultz, M. P. and Flack, K. A., The rough-wall turbulent boundary layer from the hydraulically smooth to the fully rough regime, Journal of Fluid Mechanics, Vol.580 (2007), pp.381-405.

Sinhuber, M., Bodenschatz, E. and Bewley, G. P., Decay of turbulence at high Reynolds numbers, Physical Review Letters, Vol.114, No.3 (2015), 034501.

Suzuki, H., Nagata, K., Sakai, Y. and Hayase, T., Direct numerical simulation of turbulent mixing in regular and fractal grid turbulence, Physica Scripta, Vol.2010, No.T142 (2010), 014065.

Suzuki, H., Nagata, K., Sakai, Y., Hayase, T., Hasegawa, Y. and Ushijima, T., Direct numerical simulation of fractal-generated turbulence, Fluid Dynamics Research, Vol.45, No.6 (2013), 061409.

Valente, P. C. and Vassilicos, J. C., Dependence of decaying homogeneous isotropic turbulence on inflow conditions, Physics Letters A, Vol.376, No.4 (2012), pp.510-514.

Volino, R. J., Schultz M. P. and Flack K. A., Turbulence structure in a boundary layer with two-dimensional roughness, Journal of Fluid Mechanics, Vol.635 (2009), pp.75-101.

Volino, R. J., Schultz M. P. and Flack K. A., Turbulent structure in boundary layers over periodic two- and three-dimensional roughness, Journal of Fluid Mechanics, Vol.679 (2011), pp.172-190.

Wang, H. and George, W. K., The integral scale in homogeneous isotropic turbulence, Journal of Fluid Mechanics, Vol.459 (2002), pp.429-443.

[DOI: 10.1299/jfst.2016jfst0012]